RSC Advances

ROYAL SOCIETY OF CHEMISTRY

www.rsc.org/advances

Anomalous Morphology Evolution during Stress Relaxation of Cobalt Films due to the Dissolution in Electrolyte Solutions

Tianzhi Luo,[*a, b] Lian Guo [a] and Robert C. Cammarata [*a]

[a] Department of Materials Science and Engineering, Whiting School of Engineering, Johns Hopkins University, MD 21218, USA

[b] Department of Cell Biology, School of Medicine, Johns Hopkins University, Baltimore, MD, 21205, USA

* Correspondence: T. Luo at tzluo@jhu.edu and R. C. Cammarata at rcc@jhu.edu

Abstract

The stress relaxation during the interruptions of cobalt thin film growth by electrodeposition was monitored by cantilever bending technique. The surface morphological evolution of cobalt thin films during stress relaxation was characterized by atomic force microscopy. Unlike the stress relaxation of perfect cobalt film, the relaxation of cobalt film with surface imperfections displayed irreversible characters and was suggested to be the result of cobalt dissolution in electrolytes. Additionally, the irreversible stress relaxation was accompanied by mass lost and open circuit potential change, supporting the dissolution mechanism. Scaling analysis of the morphology evolution indicated that the local stress is one of the primary driving forces for the dissolution. Additives containing Cl^- silenced the stress relaxation by improving the smoothness of film surface.

1. Introduction

Residual stress is known to be critical to the reliability and performance of devices and materials made of thin films. [1] Electrochemical deposition (ECD) has been extensively used as a massive and economic method for the production of electronics and coatings in industry. Significant amount of effort has been paid to the investigation of the stress evolution mechanisms during thin film growth by ECD. [2-9] Yet, the understanding is still incomplete because of the complexity of the solid-liquid interface and the multiplicity of the electrochemical reactions.

Cantilever technique is commonly employed to monitor the stress relaxation during the interruption of thin films growth by ECD (Fig. 1). [10, 11] For thin film growth in Volmer-Weber mode, the stress evolution displays a compression-tension-compression transition. The last compression phase is associated with the formation of continuous film. Using this technique, it has been demonstrated that the stress relaxation for a continuous film with perfect surface, is largely due to the outflow of the adatoms from the grain boundaries to the film surface. [3, 12] This type of relaxation during growth interruption has an exponential profile and is reversible in nature. Namely, the resumption of deposition led to a concave down transition of stress and the average stress in thin film eventually reached to the same level as that of before interruption of deposition (Fig. 2a). However, recent observations showed that the stress relaxation for some films grown by ECD was irreversible where the resumption of deposition resulted in a concave up transition of stress (Fig. 2b). Meanwhile, surface characterizations of these films suggested that the presence of imperfections (such as pin holes) in these films (Fig. 2c). Although researchers have reached a consensus that the driving force for the reversible stress relaxation of continuous films is the chemical potential difference between the grain boundary and the surface, it is still important to investigate whether the irreversible relaxation is related to the surface imperfections for practical purpose as the imperfections are prevail in industry products. For example, the magnetic thin films of cobalt, iron and nickel have been widely used in electromagnetic devices, such as the read-and-write head of hard drive and various field-effect devices. [13, 14] As the microstructures of these films have been shown to be critical to the magnetic properties as well as the performance of these devices, [15-19] the understanding of the imperfection-induced stress relaxation during thin film growth becomes extremely valuable. Specifically, we study the stress relaxation of cobalt thin deposited on amorphous substrates, which eliminates the preferential growth along grain boundaries on polycrystalline substrates and makes the growth cobalt islands more uniformly. The mechanisms revealed for cobalt deposition can be potentially applied to other systems.

In this study, we measured the stress relaxation of cobalt thin film deposited by ECD and characterized the surface of the films by atomic force microscopy (AFM). We proposed that the irreversible relaxation was due to the dissolution of cobalt. As dissolution is associated with mass loss, we monitored the mass change by quartz crystal microbalance (QCM). Meanwhile, we also characterized the open circuit potential (OCP) change of the films. The correlation between mass loss and OCP change strongly suggests that the irreversible stress relaxation is a result of dissolution due to the presence of surface imperfections.

2. Theory

During deposition interruption, there are only two possible reactions on the film surface: dissolution and passivation. In the electrolyte solutions, pure metals may undergo following reactions: [20]

$$M \rightarrow M^{+}_{aq} + e^{-} \quad \text{(r1)}$$

$$M + H_2O \rightarrow MOH_{ads} + H^{+} + e^{-}, \quad \text{(r2)}$$

$$MOH_{ads} \rightarrow MOH^{+}_{aq} + e^{-}, \quad \text{(r3)}$$

$$MOH_{ads} + H_2O \rightarrow M(OH)_2 + H^{+} + e^{-}, \quad \text{(r4)}$$

$$nM + mH_2O \rightarrow M_nO_m + 2mH^{+} + me^{-}, \quad \text{(r5)}$$

where M represents the metal atoms; M^{+} is the metal ion; the subscript "aq" and "ads" represent aqueous state and adsorbed state; n and m are integers. Reactions (r1), (r2), and (r3) are associated with dissolving. Reactions (r4) and (r5) are passivation. As the chemical reactions continue at the solid-liquid interface, the driving forces of all those reactions evolve as a result of the changing of ions concentration and the pH near that interface. Dissolution is associated with mass loss whereas passivation leads to mass gain. At low temperature, there is no mass change in the stress relaxation if it is induced by any physical processes, such as surface diffusion or creep. Thus, one can distinguish not only physical processes from chemical ones but also dissolution from passivation by observing the mass change if chemical reactions indeed occur. Additionally, chemical reactions involve concentration changes of ions and chemical potential changes of solids. Thus, OCP measurement can provide complementary information about whether chemical reactions occur and which reaction dominates.

Theoretical analysis has already shown that stress in films affect surface evolution during dissolution. [21-23] Consider a solid thin film, deformed by a lateral stress σ ($\sigma > 0$ for tension and $\sigma < 0$ for compression), has a surface profile $h(x,t) = h_0(t) + a(t)\cos(\omega x)$. Here, $h_0(t)$ is the average height of the surface over x; $a(t)$ is the magnitude of the cosine wave; $\omega = 2\pi/\lambda$ with λ for the wavelength of the

surface. Assuming small perturbation ($a\omega << 1$), to the first order in $a\omega$, the elastic energy density per atom is given by $w = \sigma^2(1-4a\omega\cos(\omega x))/2E$, where E is the Young's modulus of the film. According to Herring's definition, [24] the chemical potential along the surface has the form of $\mu(x) = \Omega(g_0 + \gamma\kappa + w)$, where g_0 is the chemical potential density of a flat surface without stress; γ is the interface energy; κ is the curvature at position x; Ω is the volume of single species that composes the film. With small slope approximation, the local curvature is given by $\kappa = a\omega^2\cos(\omega x)$. The growing velocity along the normal direction of surface is $R = M(g_0 + \gamma\kappa + w)$, where M is the mobility and the summation of the terms in the bracket is the driving force. For a perfect flat surface with elastic energy density w_0, the drive force is $g_0 + w_0$. [25] At this moment, only negative driving force (dissolution) is considered. Since geometrically $R = \partial h/\partial t \cdot \vec{n}$, the surface evolution can be described by $\partial h/\partial t = M(g_0 + \gamma\kappa + w)\sqrt{1+|\nabla h|^2}$, where $\vec{n}$ is the surface normal with the value $\left(\sqrt{1+|\nabla h|^2}\right)^{-1}$. Thus, one has

$$\frac{1}{a}\frac{\partial a}{\partial t} = M\left(-\gamma\omega^2 + 2\sigma^2\omega/E\right). \quad (1)$$

and

$$h(x,t) = a(0)\cos(\omega x)\exp\left[-M(t)\left(\gamma\omega^2 - 2\sigma^2\omega/E\right)t\right] + M(g_0 + w_0)t + h_0(0). \quad (2)$$

The characteristic time of the exponential term is $\tau_e^{-1} = M\left(-\gamma\omega^2 + 2\sigma^2\omega/E\right)$. The surface roughness undergoes an exponential decay with time. The average dissolution thickness is $\Delta\overline{h(t)} = M(g_0 + w_0)t$. Accordingly, the mass change is a linear function of dissolution time when the driving force does not change with time.

3. Experimental technique

3.1 Substrate Preparation

For ECD, the substrate must be conductive and inert to the electrolyte solution. Here, a very thin amorphous NiTi layer with an underlying Cr seed layer was coated on VWR 150 μm thick glass slide, serving as the working electrode. The surface roughness of the substrate characterized by AFM was smaller than 5nm.

3.2 Electrochemical deposition

The deposition cell was made of Teflon and its bottom was sealed with a quartz bottom cover that is transparent to laser beam while minimizing the laser absorption. The basic electrolyte solution in this study was $CoSO_4$ dissolved deionized (DI) water, ranging from 0.01 to 0.1 mol/L with the pH values between 4 and 7. The reference electrode was an Ag/AgCl electrode and the counter electrode was a piece of platinum plate. The electrochemical deposition was controlled by an EG&G Princeton Applied Research Corporation model 263A potentiostat/galvanostat. A constant current mode was used with the assumption of 100% cathode current efficiency.

3.3 Stress measurement

The stress was measured by cantilever bending technique (Fig. 1). The substrate and the counter electrode were mounted in a parallel fashion while the counter electrode was placed 1 cm above the substrate (working electrode/cathode). The substrate was about 1 cm away from the quartz cover. The data acquisition rate for stress signals was maintained at 10Hz. The photocurrent signals due to the bending of the substrate were converted to stress*thickness based on a pre-calibrated curve.

3.4 Characterization of thin film morphology

The film morphology was characterized by a Molecular Image PicoScan AFM. The scanning tips were made of SiN_4. The morphology after stress relaxations was measured in taping mode because of the very rough surfaces. The scan speed was below 4 lines/s to ensure the image quality. The AFM was contained in a sound-proof box that was positioned on an optical table. The images were analyzed by SPIP software (www.imagemet.com).

Scanning electron microscopy (SEM) JEOL 6700F was also used to characterize the topology of the deposited films. Chemical composition of the film surface was characterized in backscattering mode.

3.5 Mass change measurement

An Electrochemical Quartz Crystal Microbalance (Gamry instruments) was used to measure the mass change. For the dissolution measurement, the quartz substrates were coated with a thin layer of amouphous NiTi to make the substrate surface almost identical to those used for stress measurement. The mass change was correlated to the frequency change of the quartz substrates by Sauerbrey equation.

4. Results and discussion

To illustrate the irreversibility of the stress relaxation, a typical stress evolution associated with deposition interruptions after the films became continuous is shown in Fig. 2b. The insert is the complete stress signal. Before interruption, the stress evolution attained a steady state with a nearly constant slope, indicating a constant compressive stress. During interruptions, the stress signal exhibits exponential increase towards the tensile regime to release compressive stress whatever the overall stress state of the film is either tensile or compressive. After a short period of time with the resumption of deposition, the stress recovers the same slope as that before the interruption, which is similar to that observed in other systems. However, it has a concave up shape rather than a concave down profile (as indicated by the dotted line in Fig. 2b) that has been observed by others. The concave down transition in the beginning of deposition resumption together with the exponential stress relaxation have been named as reversible stress relaxation. [3, 12] It is commonly accepted that the reversible stress relaxation is due to the reversible adatom flux flowing in and out of the grain boundaries when the deposition is on and off. [10, 24] As shown in Fig. 11, the stress relaxation process during ECD can not be considered as completely reversible though the stress relaxation signal has exponential characters.

The irreversibility of the stress relaxation indicates the existence of certain dissipation process. A reasonable guess is dissolution. To test the hypothesis that the dominant mechanism for stress relaxation is a result of dissolution, mass and OCP were monitored during deposition interruptions by QCM and potentiostat, respectively. Two individual stress relaxation measurements were conducted (after long time deposition of 0.7Å/s, equivalent to 0.2 mA/cm^2) at different values of instantaneous stress of -26MPa and -58MPa for Co deposition in 0.05 mol/l $CoSO_4$ (pH~4.4), shown in Fig. 3a and b, respectively. The energy relaxations are about 2GPa·Å. The magnitudes of OCP transients measured relatively to saturated hydrogen electrode (SHE) are about 0.3 V. After 50~100s period of significant varying, the OCP almost reaches a constant value eventually. The mass change measurement is shown in Fig. 3c. It is evident that the mass (frequency signal) varies linearly with time, which is consistent with the theoretical predication based on Eq. 2. Even for long time scale, for example 30 minutes, the mass change still remained a linear profile (not shown).

Under open circuit condition, the significant change of OCP indicates that certain chemical reactions were associated with stress relaxation. Amorphous NiTi substrates have an equilibrium potential about 0.26V to SHE. The mixed oxides (mainly TiO_x) have much higher equilibrium potential than that of NiTi alloy. The equilibrium potential of Co is -0.28V to SHE. According Pourbiax diagrams, [26] if the oxide

layer is effectively exposed to the electrolyte solutions, galvanic corrosion will occur and the films will be dissolved into solution while the OCP will change from the value of corresponding film to that of the substrate. The existence of pin-holes in electrochemically deposited films has been reported repeatedly in literatures. These pin-holes can sometimes form 3D connected network from the bottom to the surface of the films and thus provide a channel for the substrates to contact the electrolyte solutions, which allows the galvanic corrosion to take place. Indeed, in SEM measurements (backscattering mode with chemical composition analysis), holes were observed frequently for the deposited cobalt films (Fig. 2c). Meanwhile, the magnitude of OCP change observed in our experiments (Fig. 3) was 0.3 V, which is very close to the theoretical equilibrium difference between Co and NiTi, 0.4 V. The significant change of OCP also rules out the possibility of passivation of cobalt where OCP change is only about 0.02 V. [27]

Based on above analysis and experimental evidence, it is highly possible that the dominant mechanism for stress relaxation observed in my experiments is dissolution (galvanic corrosion) if the substrates effectively contact the electrolytes through the network of pin-holes. Although surface diffusion of adatoms and back flow of adatoms from grain boundaries do play important roles in morphology change during dissolution, their physical nature of these processes cannot explain the significant OCP change and mass change that are the inherent characters of chemical processes.

It is known that stress plays important role in surface evolution. Enormous amount of theoretical analysis and experiments have studied the morphology evolution of a solid surface which was deformed by constant loading. [21-23, 28-30] In our experiments, the stress is self-generated and its magnitude varies with time. To investigate how the stress affects the surface evolution during deposition interruption, the surfaces of Co films at different dissolution periods were characterized in tapping mode by AFM. The images of t=0, 20, and 100 seconds are presented in Fig. 4a. All the images have the size of $10\times10\mu m^2$ and the pixels of 512×512. The height-height correlation function, $H(r)=\left\langle[h(\vec{r})-h(0)]^2\right\rangle$, is often used to describe the surface morphology in statistics sense. The common scaling hypothesis states that $H(r)\propto r^{2\alpha}$ for $r<<\xi$ and $H(r)\propto 2w^2$ for $r>>\xi$, where ξ is the correlation length, w is the surface roughness and α is the roughness exponent. [31, 32] The corresponding height-height correlation function of the AFM images in Fig. 2 is calculated along the fast scanning direction by [33]

$$H(r)=H(m)\approx\frac{1}{N_y(N_x-m)}\sum_{l=1}^{N_y}\sum_{n=1}^{N_x-m}[z(m+n,l)-z(n,l)]^2 \qquad (3)$$

where $N_x = N_y = 512$, m and n is integers, $z(n,l)$ is the height of the pixel at position (n,l). The results are drawn in a log-log plot in Fig. 4b, suggesting that the surface morphology was self-affine and all height-height correlation functions had the roughness exponent α. The surface roughness parameters w , ξ and α can be obtained by fitting the height-height correlation functions to $H(r) = 2w^2\left[1 - \exp\left(-(r/\xi)^{2\alpha}\right)\right]$. It was found that the roughness exponent α was about 0.7 ± 0.025 for all the images. The surface roughness and correlation length are plotted in Fig. 4c. The surface roughness decayed over time.

As the growth process of thin films grown by ECD shares many similarities with that by molecular beam epitaxy (MBE), one might be able to qualitatively analyze the effect of stress effect on the roughening during electrodeposition or electrodissolution using the knowledge of kinetic roughening of MBE. The corresponding equation describing the surface roughening under stress is [34]

$$\frac{\partial h}{\partial t} = -\zeta\nabla^4 h + \psi\nabla^3 h + F + \eta(\vec{r},t), \qquad (4)$$

where ψ is a parameter depending on the elastic energy density of the diffusion species on the surfaces. Here, F represents either the deposition rate or the dissolution rate. From the scaling theory one knows that $\alpha = (4-d)/2$ if the first term at the righthand side dominates and $\alpha = (3-d)/2$ if the second term dominates. Here, d is the dimension of the system under study. For thin film growth, one has $d = 2$ and $1/2 \le \alpha \le 1$. Based on the experimental evidence in Fig. 3, it is reasonable to describe the stress relaxation behavior by

$$\sigma(t) = \sigma_i + (\sigma_f - \sigma_i)\left[1 - \exp(-t/\tau_r)\right], \qquad (5)$$

where τ_r is the characteristic relaxation time, σ_i and σ_f is the initial and final stress states during stress relaxation, respectively. Since $\psi(\sigma(t)) \propto \sigma(t)^2$, one expects ψ also varies exponentially with time more or less.

As shown in Fig. 3, the typical stress relaxation and associated OCP changes have a characteristic relaxation time τ_r, about 60 s. It is noticed that the roughness parameters did show different behaviors before and after 60s. Additionally, the roughness exponent α in this study is more close to $1/2$, indicating the surface evolution is stress dominated rather than surface diffusion governed. Therefore, surface evolution during dissolution is strongly dependent on the stress evolution.

The purpose of introducing Eq. (4) in scaling analysis is to emphasize that stress can not be ignored if its magnitude is significant. One thing needs to mention is that the stress measured in experiments is the average or overall stress of the whole film while the stress in Eq. (4) is more relevant to the local stress near the surface. [21-23, 28-30] Most of thin films grown by ECD are polycrystalline films. It is well known that stress near the groovings (grain boundaries) is dramatically different from that near the top of the mounds on the film surfaces, which makes it very challenging to make quantitative analysis and discussions. Additionally, a second order derivative term $\chi\nabla^2 h$ should also be introduced to represent the laplacian fields, such as the electrical field for certain cases. [35]

Additives have been commonly used to improve the surface quality of the films grown by ECD. Adding the supporting electrolyte not only changes the double layer structure of solid-liquid interface but also changes the diffusivity of the metallic ions. It is well known that anions like Cl^- can form adsorption layer on metal surfaces, such as Cu(111), Pt(111) and Au(111). Although there is no available literature about whether and how the Cl^- are adsorbed on Co(111), it is suspected there is great chance that the adsorption of those ions on Co surface also occurs. [36]

To investigate whether the irreversible stress relaxation still occurs in the presence of the additives, the stress evolutions of $CoSO_4$ with the addition of different amount of NaCl were characterized. In Fig. 5, Stress evolutions at deposition rate of 0.7 Å/s (equivalent to 0.2mA/cm^2) are shown for 0.05mol/l $CoSO_4$ with addition of 0.01 and 0.1 mol/l NaCl. In comparison to the cases without additives (Fig. 2 and 3), the magnitude of the stress relaxation was negligible. It has been reported that the presence of small anions resulted in reduced grain size in Copper film depositions. [36] We suspect that similar mechanism may operate in Cobalt film depositions here. In fact, AFM images showed that Cobalt deposition with Cl^- displayed islands with 35nm in height and 1 μm^2 base whereas the deposition in the absence of Cl^- produced islands with similar height but 0.2 μm^2 base (Fig. 6). This suggests that the addition of Cl^- results in flatter grains. As a result, the surface of Cobalt films becomes much smoother and has less pin-holes, which minimizes the irreversible stress relaxation due to dissolution. The reduced height/base ratio presumably leads to earlier island-coalescence and smaller critical film thickness where films become continuous. This is supported by the facts that tensile stress peaks had lower magnitude and occurred earlier with the addition of Cl^- (Fig. 5) than those in the absence of Cl^- (Fig 2.) at the same deposition rate since the amount of tensile stress is proportional to the height of grain before the formation of continuous film. [37, 38] Additionally, we did not find pin-holes in the SEM images of the Cobalt films deposited with

the addition of Cl^-. Therefore, smaller anions, such as Cl^-, are able to protect the films from dissolution (or corrosion attack) and maintain the growth stress.

5. Conclusions

In situ stress measurements were performed for Co electrochemical deposition on amorphous substrates with and without supporting electrolyte. Unlike the stress relaxation of perfect cobalt film, the relaxation of cobalt film with surface defects (such as pin-holes) displayed irreversible characters. Additionally, the irreversible stress relaxation was accompanied by mass lost and open circuit potential change, supporting the dissolution mechanism. Scaling analysis of the morphology evolution suggested that the local stress is one of the primary driving forces for the dissolution. Additives containing Cl^- silenced the stress relaxation by improving the smoothness of film surface. Taken together, the surface imperfections are required and the intrinsic stress inside films is necessary for the dissolution induced irreversible stress relaxation to occur during deposition interruption. The mechanisms revealed for Co deposition under constant current condition might be used for other systems.

Acknowledgments

The authors gratefully acknowledge the extremely valuable help from Prof. Karl Sieradzki and Dr. Lei Tang. Support for this work from the National Science Foundation, award number DMR 0706178, is also gratefully acknowledged.

References

1. R. Koch, *J. Phys.: Condens. Matter*, 1994, **6**, 9519-9550.
2. S. J. Hearne and J. A. Floro, *J. Appl. Phys.*, 2005, **97**, 014901.
3. E. Chason, J. W. Shin, S. J. Hearne and L. B. Freund, *J. Appl. Phys.*, 2012, **111**, 083520.
4. T. Z. Luo, L. Guo and R. C. Cammarata, *J Cryst. Growth*, 2010, **312**, 1267-1270.
5. M. C. Lafouresse, U. Bertocci, C. R. Beauchamp and G. R. Stafford, *J. Electrochem. Soc.*, 2012, **159**, H816-H822.
6. M. C. Lafouresse, U. Bertocci and G. R. Stafford, *J. Electrochem. Soc.*, 2013, **160**, H636-H643.
7. G. R. Stafford and U. Bertocci, *J. Phys. Chem. B*, 2006, **110**, 15493-15498.
8. G. R. Stafford and U. Bertocci, *J. Phys. Chem.C*, 2007, **111**, 17580-17586.
9. O. E. Kongstein, U. Bertocci and G. R. Stafford, *J. Electrochem. Soc.*, 2005, **152**, C116-C123.
10. E. Chason, B. W. Sheldon, L. B. Freund, J. A. Floro and S. J. Hearne, *Phys. Rev. Lett.*, 2002, **88**, 156103.
11. C. Friesen and C. V. Thompson, *Phys. Rev. Lett.*, 2002, **89**, 126103.
12. J. W. Shin and E. Chason, *Phys. Rev. Lett.*, 2009, **103**, 056102.
13. S. S. P. Parkin, M. Hayashi and L. Thomas, *Science*, 2008, **320**, 190-194.
14. D. Chiba, M. Kawaguchi, S. Fukami, N. Ishiwata, K. Shimamura, K. Kobayashi and T. Ono, *Nat. Commun.*, 2012, **3**, 888.
15. J. L. Bubendorff, E. Beaurepaire, C. Mény, P. Panissod and J. P. Bucher, *Phys. Rev. B*, 1997, **56**, R7120-R7128.
16. A. Gundel, L. Cagnon, C. Gomes, A. Morrone, J. Schmidt and P. Allongue, *Phys.Chem. Chem. Phys.*, 2001, **3**, 3330-3335.
17. Y.-L. Chan, Y.-J. Hung, C.-H. Wang, Y.-C. Lin, C.-Y. Chiu, Y.-L. Lai, H.-T. Chang, C.-H. Lee, Y. J. Hsu and D. H. Wei, *Phys. Rev. Lett.*, 2010, **104**, 177204.
18. D. Hunter, W. Osborn, K. Wang, N. Kazantseva, J. Hattrick-Simpers, R. Suchoski, R. Takahashi, M. L. Young, A. Mehta, L. A. Bendersky, S. E. Lofland, M. Wuttig and I. Takeuchi, *Nat. Commun.*, 2012, **2**, 518.
19. A. Berger, O. Idigoras and P. Vavassori, *Phys. Rev. Lett.*, 2013, **111**, 190602.
20. P. Marcus, *Corrosin Mechanisms in Theory and Practice*, 2nd edn., CRC Press, Boca Raton, USA, 2002.
21. R. J. Asaro and W. A. Tiller, *Metall. Trans.*, 1972, **3**, 1789-1796.
22. M. A. Grinfeld, *Soviet Phys. Doklady*, 1986, **31**, 831-834.
23. D. J. Srolovitz, *Acta Metall.*, 1989, **37**, 621-625.
24. C. Herring, *J. Appl. Phys.*, 1950, **21**, 437-445.
25. K. S. Kim, J. A. Hurtado and H. Tan, *Phys. Rev. Lett.*, 1999, **83**, 3872-3875.
26. P. Pourbaix, ed., *Atlas of electrochemical equilibria in aqueous solutions*, NACE International, Houston, USA, 1974.
27. W. A. Badawy, F. M. Al-Kharafi and J. R. Al-Ajmi, *J. Appl.Electrochem.*, 2000, **30**, 693-704.
28. H. H. Yu and Z. Suo, *Acta Mater.*, 1998, **47**, 77-88.
29. W. H. Yang and D. J. Srolovitz, *J. Mech.Phys. Solids*, 1994, **42**, 1551-1574.
30. J. Müller and M. Grant, *Phys. Rev. Lett.*, 1999, **82**, 1736-1739.
31. A.-L. Barabási and H. E. Stanley, eds., *Fractal concepts in surface growth*, Cambridge University Press, Cambridge, England, 1995.

32. P. Meakin, ed., *Fractals, scaling and growth far from equilibrium*, Cambridge University Press, Cambridge, England, 1999.
33. H. N. Yang, Y. P. Zhao, A. Chan, T. M. Lu and G. C. Wang, *Phys. Rev. B*, 1997, **56**, 4224-4232.
34. D. E. Wolf and J. Villain, *Europhys. Lett.*, 1990, **13**, 389-394.
35. A. Iwamoto, T. Yoshinobu and H. Iwasaki, *Phys. Rev. Lett.*, 1994, **72**, 4025-4028.
36. G. Carneval and J. B. de Cusminsky, *J. Electrochem. Soc.*, 1981, **128**, 1215-1221.
37. R. C. Cammarata, T. M. Trimble and D. J. Srolovitz, *J. Mater. Res.*, 2000, **15**, 2468-2474.
38. W. D. Nix and B. M. Clemens, *J. Mater. Res.*, 1999, **14**, 3467-3473.

Figure Caption

Figure 1. Cantilever technique for the stress measurement for thin films grown by electrochemical deposition.

Figure 2. Typical stress evolution during thin film growth under constant current condition: (a) A scheme graph of a reversible stress relaxation during the interruption of film growth, exhibiting an exponent relaxation and displaying a concave down shape after the film deposition is resumed. The stresses (slopes indicated by the triangles) before and after interruption are the same if deposition rate is maintained the same; (b) An irreversible stress relaxation observed in experiment showed a concave up shape after the resumption of deposition (for comparison, a dotted line with a concave down shape is shown). The inset is the full curve observed in experiment, displaying an exponential-like relaxation; (c) Pin-holes (black dots) was observed on the cobalt film surface by SEM.

Figure 3. Stress•thickness transients and open circuit potential transients during interruption of Co electrochemical deposition with deposition rate of 0.7 Å/s (or equivalently 0.2 mA/cm^2 current) and different instantaneous stress: (a) 26MPa; (b) 58MPa in 0.05mol/l $CoSO_4$ (pH~4.4). Mass change and associated open circuit potential transient relative to saturated hydrogen electrode (SHE) are shown in (c).

Figure 4. The surface morphology change of Co thin film during dissolution: (a) AFM images of the surface morphology of Co thin films at different relaxation time t=0, 20, and 100 s. All the images have the same size of 10×10μm^2; (b) The height-height correlation functions H as a function of the distance r is plotted for the AFM images in (a). H and r have the dimension of nm^2 and nm, respectively; (c) The roughness w and correlation length ξ for AFM images in (a). The concentration of $CoSO_4$ was 0.05mol/l.

Figure 5. Stress evolution of films deposited in the solution of 0.05mol/l $CoSO_4$ with 0.01 mol/l (a) and 1.0 mol/l (b) NaCl at deposition rate of 0.7 Å/s (or equivalently 0.2 mA/cm^2 current). The interruption periods are indicated by arrows.

Figure 6. AFM images of Cobalt deposition at the deposition rate of 0.7 Å/s (or equivalently 0.2 mA/cm^2 current) in 0.05mol/l $CoSO_4$ without (a) and with (b) 0.01 mol/l NaCl at a duration of 50 s. The grain height in both (a) and (b) is about 35nm.

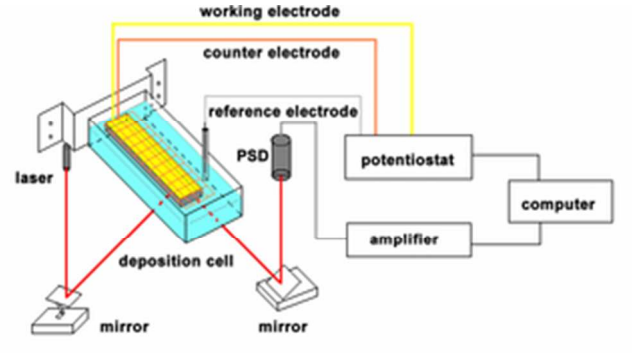

Cantilever technique for the stress measurement for thin films grown by electrochemical deposition.
26x14mm (300 x 300 DPI)

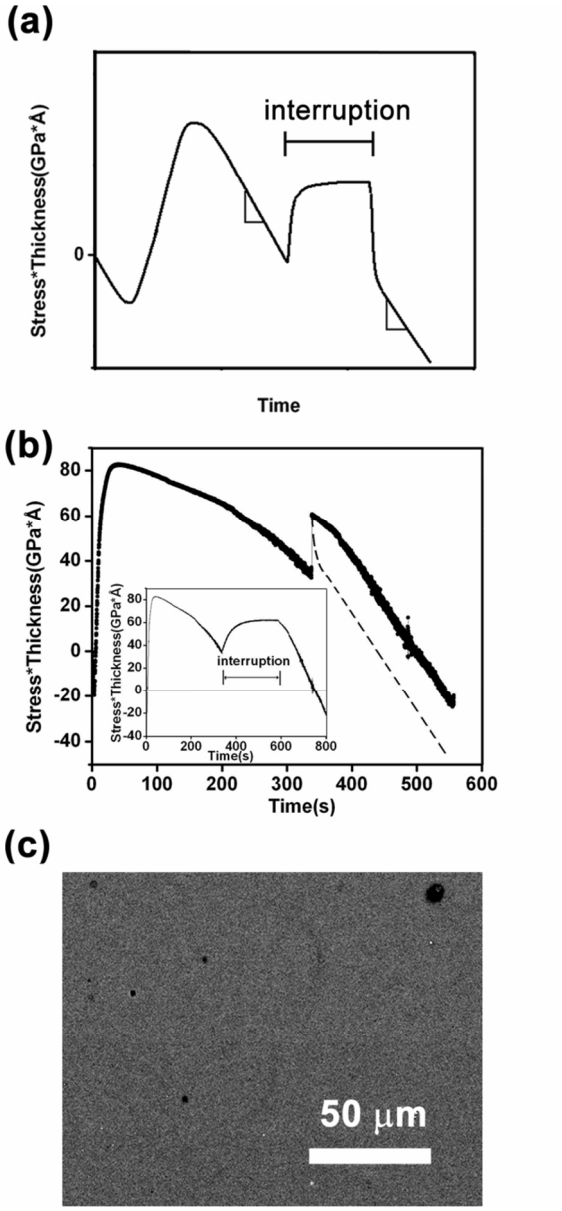

Typical stress evolution during thin film growth under constant current condition: (a) A scheme graph of a reversible stress relaxation during the interruption of film growth, exhibiting an exponent relaxation and displaying a concave down shape after the film deposition is resumed. The stresses (slopes indicated by the triangles) before and after interruption are the same if deposition rate is maintained the same; (b) An irreversible stress relaxation observed in experiment showed a concave up shape after the resumption of deposition (for comparison, a dotted line with a concave down shape is shown). The inset is the full curve observed in experiment, displaying an exponential-like relaxation; (c) Pin-holes (black dots) was observed on the cobalt film surface by SEM.
66x139mm (300 x 300 DPI)

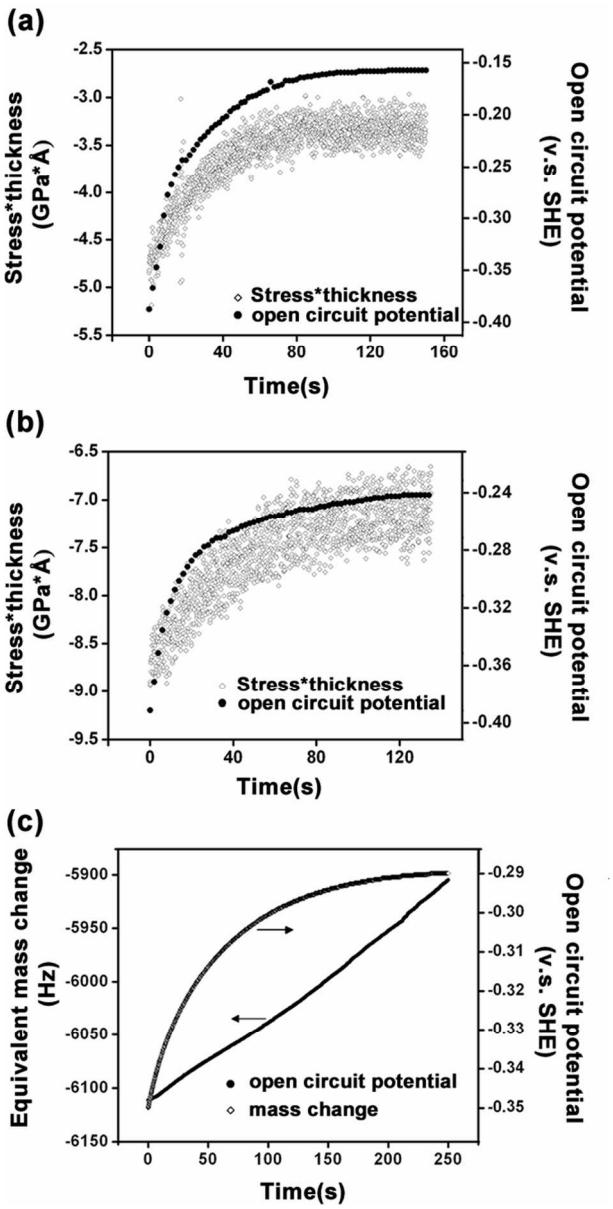

Stress•thickness transients and open circuit potential transients during interruption of Co electrochemical deposition with deposition rate of 0.7 Å/s (or equivalently 0.2 mA/cm2 current) and different instantaneous stress: (a) 26MPa; (b) 58MPa in 0.05mol/l CoSO4 (pH~4.4). Mass change and associated open circuit potential transient relative to saturated hydrogen electrode (SHE) are shown in (c).
62x123mm (300 x 300 DPI)

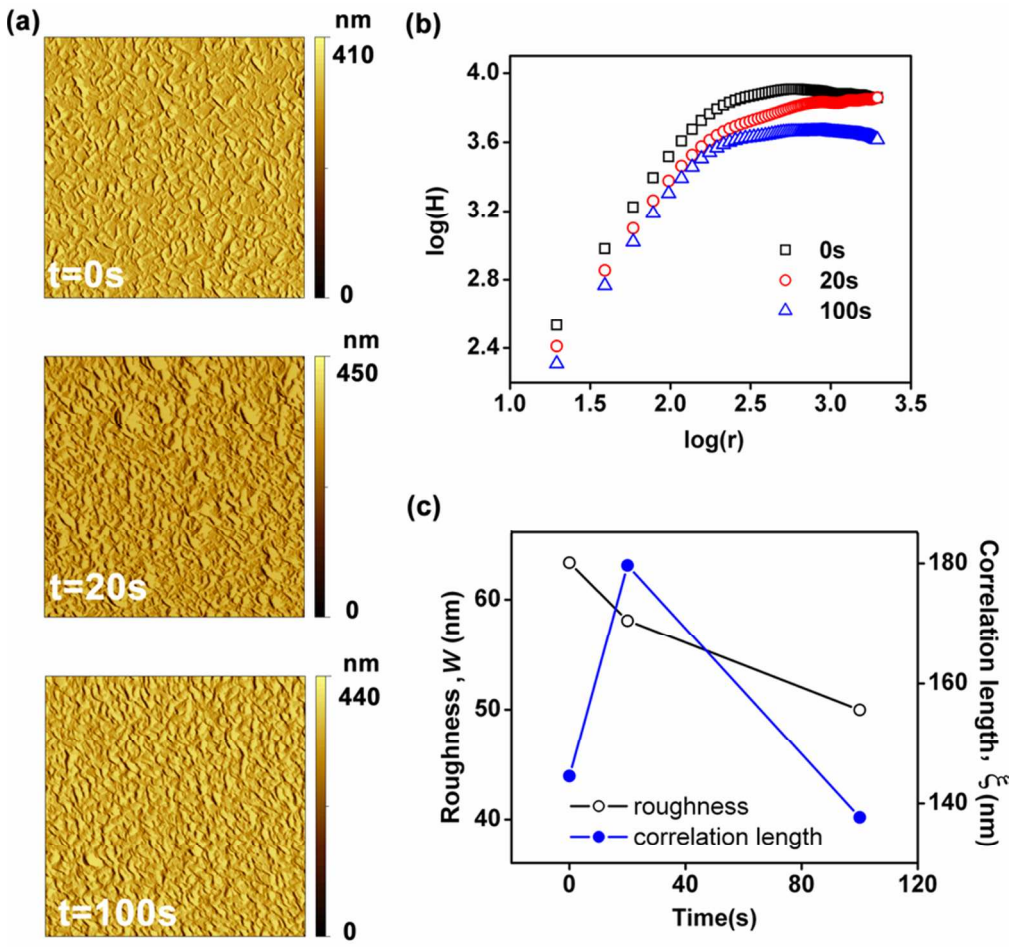

The surface morphology change of Co thin film during dissolution: (a) AFM images of the surface morphology of Co thin films at different relaxation time t=0, 20, and 100 s. All the images have the same size of 10×10μm2; (b) The height-height correlation functions H as a function of the distance r is plotted for the AFM images in (a). H and r have the dimension of nm2 and nm, respectively; (c) The roughness and correlation length for AFM images in (a). The concentration of CoSO4 was 0.05mol/l.
79x74mm (300 x 300 DPI)

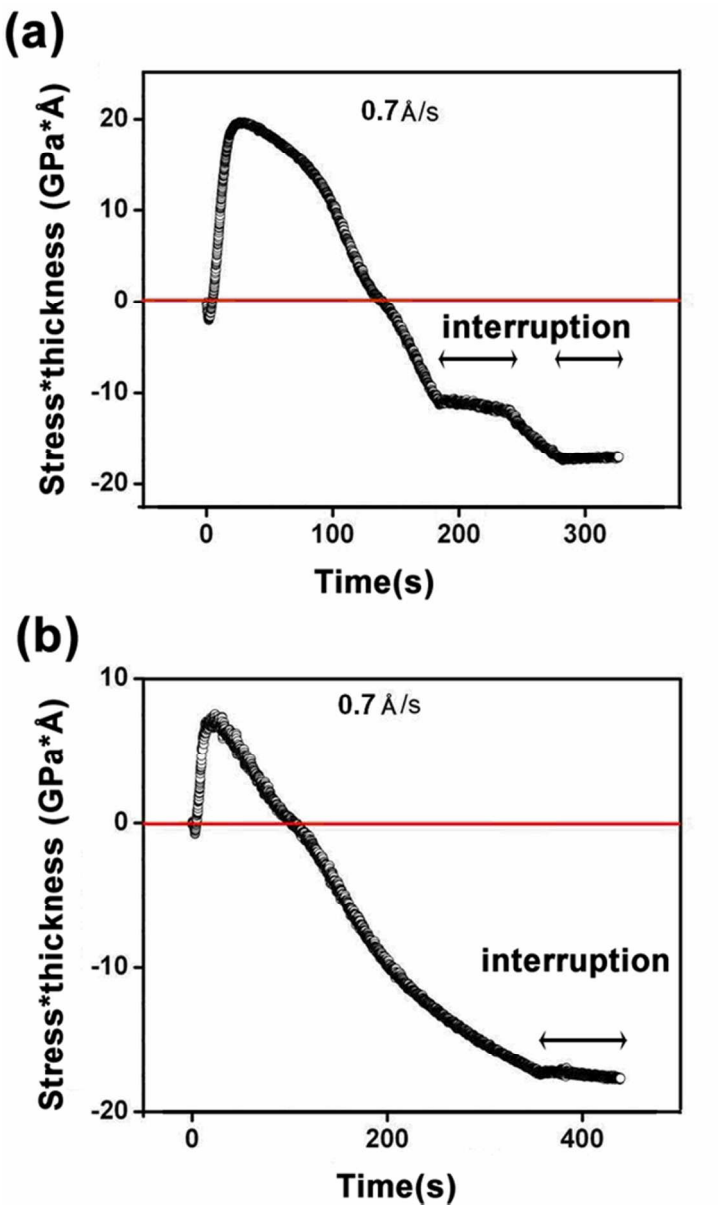

Stress evolution of films deposited in the solution of 0.05mol/l CoSO4 with 0.01 mol/l (a) and 1.0 mol/l (b) NaCl at deposition rate of 0.7 Å/s (or equivalently 0.2 mA/cm2 current). The interruption periods are indicated by arrows.
50x84mm (300 x 300 DPI)

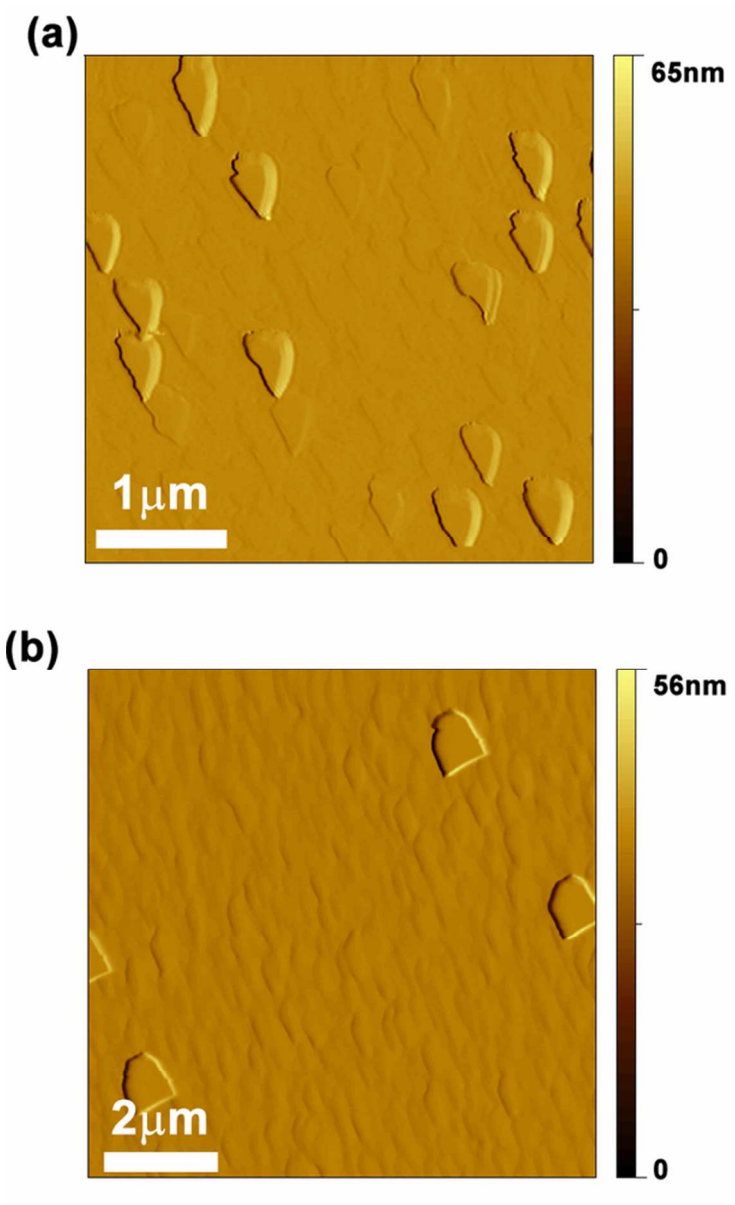

AFM images of Cobalt deposition at the deposition rate of 0.7 Å/s (or equivalently 0.2 mA/cm2 current) in 0.05mol/l CoSO4 without (a) and with (b) 0.01 mol/l NaCl at a duration of 50 s. The grain height in both (a) and (b) is about 35nm.
51x84mm (300 x 300 DPI)

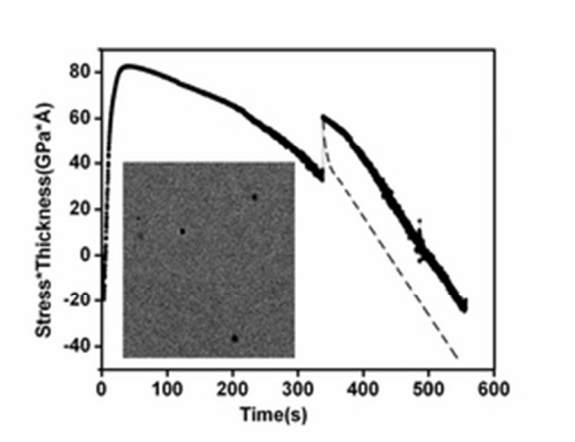

Unlike the stress relaxation of perfect cobalt film (the dotted cure), the relaxation of cobalt film with surface imperfections (such as black pin-holes in above insert) displayed irreversible characters and was suggested to be the result of cobalt dissolution in electrolytes, which could be eliminated by additives such as Cl-.
24x18mm (300 x 300 DPI)